JACS
JOURNAL OF THE AMERICAN CHEMICAL SOCIETY
Article
pubs.acs.org/JACS

Investigating the Dearomative Rearrangement of Biaryl Phosphine-Ligated Pd(II) Complexes

Phillip J. Milner, Thomas J. Maimone,† Mingjuan Su, Jiahao Chen, Peter Müller, and Stephen L. Buchwald*

Department of Chemistry, Massachusetts Institute of Technology, Cambridge, Massachusetts 02139, United States

Supporting Information

ABSTRACT: A series of monoligated L·Pd^{II}(Ar)X complexes (L = dialkyl biaryl phosphine) have been prepared and studied in an effort to better understand an unusual dearomative rearrangement previously documented in these systems. Experimental and theoretical evidence suggest a concerted process involving the unprecedented Pd^{II}-mediated insertion of an aryl group into an unactivated arene.

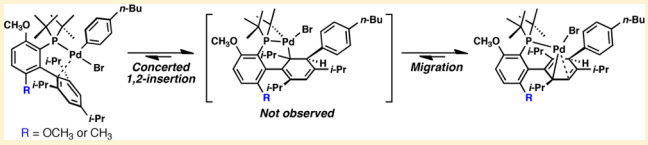

1. INTRODUCTION

Dialkyl biaryl phosphine ligands have seen application in a variety of Pd-catalyzed cross-coupling reactions, including those forming C–C,[1] C–N,[2] C–O,[3] C–CF$_3$,[4] and C–X (X = F, Cl, Br)[5] bonds. Catalysts based on derivatives of 2-(di-*tert*-butylphosphino)biphenyl (JohnPhos, **1**),[6] such as SPhos (**2**),[1a,d,7] RuPhos (**3**),[2] XPhos (**4**),[1b,8] *t*BuXPhos (**5**),[1e,f,9] Me$_4$*t*BuXPhos (**6**),[3c,9f,10] BrettPhos (**7**),[2,4,11] *t*BuBrettPhos (**8**),[5,12] AdBrettPhos (**9**),[13] and RockPhos (**10**),[3b] have demonstrated particular proficiency in these reactions (Figure 1). Biaryl phosphine ligands have also proven effective in the preparation of a number of transition metal complexes, the structures of which have revealed that the non-phosphine-containing (lower) aromatic ring often serves as an additional site for binding to the metal center.[14]

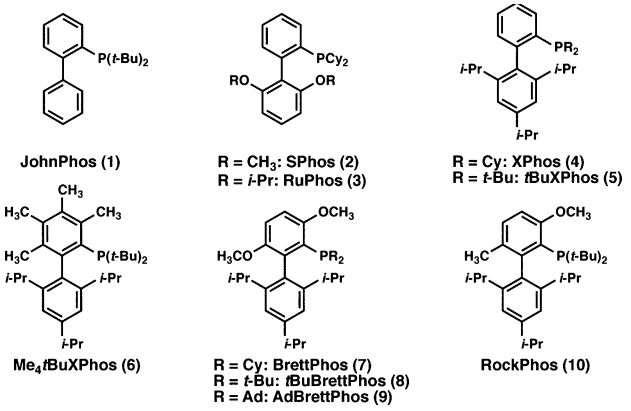

Figure 1. Biaryl phosphine ligands. Ad = adamantyl.

While studying the Pd-catalyzed conversion of aryl triflates to aryl fluorides,[5a] we discovered an unexpected rearrangement of the oxidative addition complex **11a** that established an equilibrium (K_{eq} = 5.71 ± 0.10, CD_2Cl_2) between **11a** and dearomatized **11b** (Figure 2) at room temperature.[15] The analogous complex **12a** derived from **10**, which differs only in the substitution of a methyl group for a methoxy group, was also found to undergo rearrangement to **12b**, albeit to a much lesser degree (K_{eq} = 0.08, CD_2Cl_2). Treatment of the **11a**/**11b** equilibrium mixture with 1,8-diazabicyclo[5.4.0]undec-7-ene (DBU) in the presence of 4-*n*-BuPhBr generated **13**, the oxidative addition complex of 3′-arylated *t*BuBrettPhos, presumably via a L·Pd(0) intermediate (Figure 3).

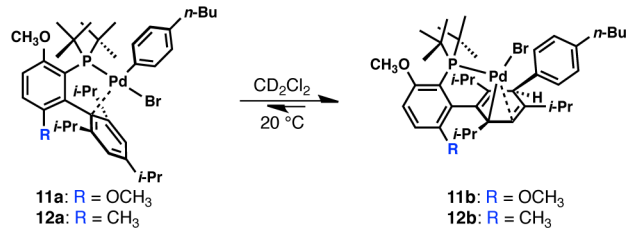

Figure 2. Rearrangement of **11a** to **11b**.

The arene-binding interaction observed in complexes of biaryl phosphine ligands could, in principle, facilitate dearomatization if enough weakening of the aromatic character of the lower ring occurred. Accordingly, other dearomatized

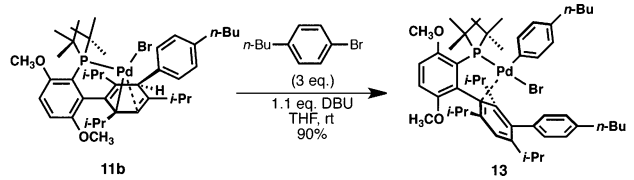

Figure 3. Elimination of **11b** with base to give **13** after oxidative addition.

Received: October 19, 2012
Published: November 15, 2012

   dx.doi.org/10.1021/ja310351e | J. Am. Chem. Soc. 2012, 134, 19922–19934

biaryl phosphine-ligated transition metal complexes have been recently reported. Prior to our work, Doyle reported a dearomatized 7-ligated Ni(II) complex (**14**),[16] and recently Allgeier and Shaw reported the decomposition of a *t*BuXPhos complex to give **15**, purportedly by a carbene insertion mechanism originating from dichloromethane (Figure 4).[17] In

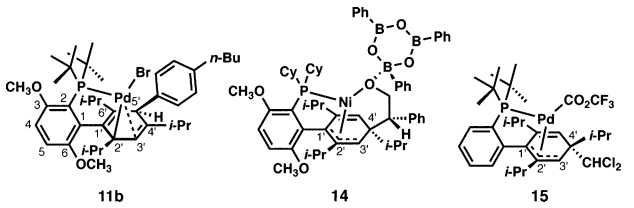

Figure 4. Recently reported dearomatized biaryl phosphine-ligated metal complexes.

both of these cases, dearomatization occurs at the 4′-position of the lower arene (see Figure 4), whereas **11b** shows a different connectivity that allows for the loss of HBr and rearomatization to occur. Taken together, these reports suggest that the lower ring of biaryl phosphine ligands may not be innocent in the reactivity and decomposition pathways of catalytic intermediates.

Reactions wherein a transition metal-bound arene undergoes nucleophilic attack are well-established,[18] as are a number of dearomatization reactions using Pd and Pt catalysts.[19] However, the reversible rearrangement of **11a**/**11b**, which formally represents an aryl migratory insertion into an aromatic ring, is quite unusual. Concerted aryl migratory insertion processes from Pd(II) have been proposed as a potential pathway in a large number of C−H arylation reactions,[20] but little is known experimentally about the viability of this process, and the direct observation of the product of the insertion of an aryl group into an aromatic ring from Pd(II) had never, to our knowledge, been reported prior to our work. Likewise, the reverse of this process would represent a rare example of β-aryl elimination from an isolated Pd(II) complex.[21,22] Due to the increasing number of reports concerning dearomatization reactions of biaryl phosphine-ligated complexes, the importance of these ligands in difficult cross-coupling reactions, and the possible relevance of the mechanism of this process to those of C−H arylation reactions,[20] we set out to investigate the mechanistic features of this rearrangement both experimentally and computationally.

Several possible mechanisms for the rearrangement of **11a** to **11b** are shown in Scheme 1. Numerous mechanistic studies of aryl migratory insertions into alkenes using bidentante ligands or small monodentate ligands have been conducted.[23] Most relevant to this study, Brown found that intramolecular migratory insertions of electron-rich Pd(II) complexes are incredibly facile, and with monodentate phosphine ligands the insertion most likely proceeds directly from the L·Pd(aryl)X-(alkene) species.[24] In the solid-state structure of **11a**, the aryl group and lower ring of the ligand are *trans*, but a concerted insertion requires the π system and migrating groups to be *cis*. Therefore, isomerization (possibly by pseudo-rotation of a tricoordinate 14-electron Pd-species) to *cis*-**11a**′ must occur before a concerted 1,4-migratory insertion into the arene (Pathway I) or a concerted 1,2-migratory insertion to form **16** followed by a 1,3-allylic shift (Pathway II). Several cationic mechanisms (Pathways III−IV), wherein halide disassociation

Scheme 1. Plausible Pathways (I−IV) for the Rearrangement of 11a to 11b

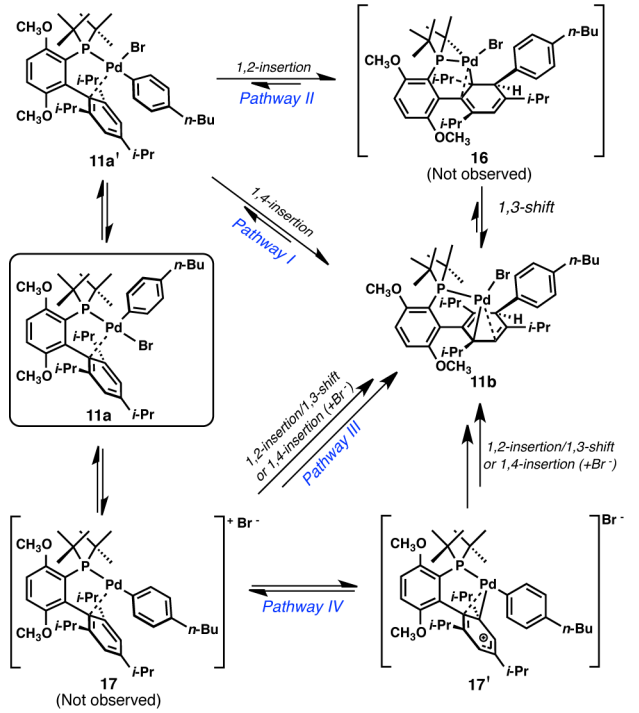

to **17** precedes 1,2- or 1,4-migratory insertion (III) as from **11a**′, or Friedel−Crafts-type electrophilic palladation to give **17**′ followed by 1,2- or 1,4-aryl migration (IV), could also be envisioned (Scheme 1).[25] With these mechanistic possibilities in mind, we investigated the effect of solvent, halide, aryl substituent, and ligand structure on the rate and extent of rearrangement to determine which pathway is most likely operative in the dearomatization of **11a**.

2. EXPERIMENTAL STUDIES

2.1. Activation Parameters. The activation parameters for the rearrangement of **11a** to **11b** were determined by Eyring analysis (10−42 °C, CD_2Cl_2, Supporting Information, Figure S2) to be $\Delta H^{\ddagger}$ = 22.1 ± 1.3 kcal/mol, $\Delta S^{\ddagger}$ = 16 ± 4 cal/K·mol, and $\Delta G^{\ddagger}$ (20 °C) = 17.4 ± 1.3 kcal/mol. The positive entropy of activation suggests that extensive reorganization of the species going to the rate-determining transition state is not necessary (*vide infra*). These parameters could be consistent with any of the mechanistic scenarios shown in Scheme 1.

2.2. Solvent Effects. The ^{31}P NMR spectrum of **11a** displays only one resonance; however, it is unusually broad, especially when compared to the analogous complex **12a** bearing the structurally similar RockPhos ligand (Figure 5). The broad ^{31}P NMR resonance of **11a** is indicative of multiple rapidly equilibrating species being present in solution, consistent with the presence of both **11a** and **11a**′. However, low-temperature (−80 °C) decoalescence and NOESY NMR experiments could not definitively establish the identity of the species present in solution (see Supporting Information).

Solvent effects on the rate and extent of rearrangement of **11a** to **11b** were also examined (Table 1). The relative rates of isomerization (k_{f+r}) and equilibrium (K_{eq}) constants were determined in THF-d_8, C_6D_6, dioxane-d_8, and CD_2Cl_2.[26] From these two parameters, the k_f rate constants for the forward rearrangement process could be determined. These findings

dx.doi.org/10.1021/ja310351e | J. Am. Chem. Soc. 2012, 134, 19922−19934

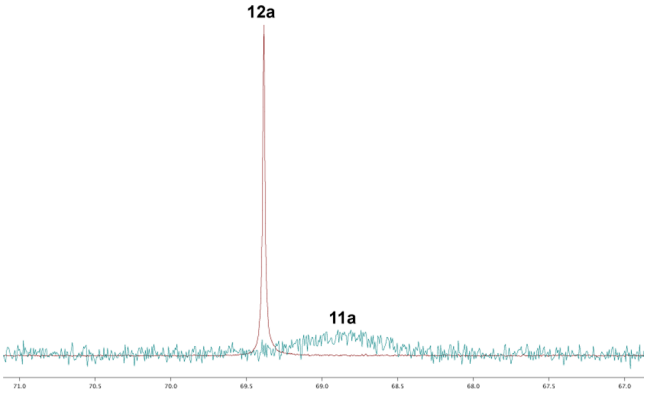

Figure 5. ^{31}P NMR (CD_2Cl_2) comparison of **11a** and **12a**.

Table 1. Solvent Effects on Rearrangement

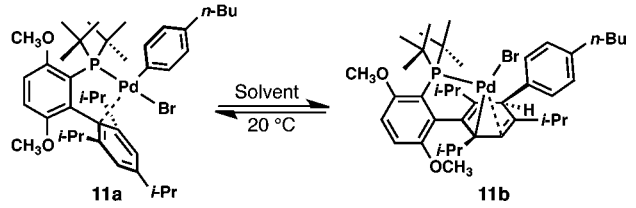

solvent	k_{f+r}[a]	k_f[a]	K_{eq}	ΔG_{exp} (kcal/mol)
CD_2Cl_2	1.22 ± 0.06	1.16 ± 0.05	5.71 ± 0.10	−1.01 ± 0.01
THF-d_8	1.00 ± 0.03	1.00 ± 0.03	8.71 ± 0.15	−1.26 ± 0.01
C_6D_6	1.44 ± 0.04	1.50 ± 0.06	13.5 ± 0.24	−1.51 ± 0.01
dioxane-d_8	1.14 ± 0.04	1.18 ± 0.04	13.5 ± 0.24	−1.51 ± 0.01

[a]Relative to **11a** in THF-d_8.

suggest that solvation has a minor effect on the relative stabilities of **11a** and **11b**, yet there is no discernible trend between solvent polarity and equilibrium concentration or rate of rearrangement. Because halide dissociation must be rate-determining or precede the rate-determining step in Pathways III and IV, these results are inconsistent with an ion-dissociation pathway, which previous studies suggest should be uniformly accelerated by more coordinating solvents such as THF and dioxane.[23d] The observation that the addition of 5 equiv of soluble Br^- (Bu_4NBr) did not decrease the rate of rearrangement is also consistent with this premise.[23d]

2.3. Aryl Substituent Effect. A range of *para*-substituted aryl bromide oxidative addition complexes based on **8** were synthesized in good isolated yields (Table 2). The kinetic profiles for the rearrangements of these species are shown in Figure 6, and the parameters corresponding to these profiles are shown in Table 3. A Hammett plot of the K_{eq} values in Table 3 was linear, yielding $\rho = -2.56 \pm 0.13$ (Figure 7).[27] Only with substituents that are electron-withdrawing by both resonance and induction (**24a**, **25a**) is the oxidative addition complex lower in energy than its dearomatized isomer. Because the aryl group is bound to a sp^3-hybridized carbon in the dearomatized complex, but interacts directly with the Pd center in the corresponding oxidative addition complexes, its identity should be of more consequence to the stability of **11,18−25a** than to **11,18−25b**; that is, electron-donating substituents must destabilize oxidative addition complexes of **8** relative to their dearomatized counterparts. The solid-state structures of **11a**, **20a**, **22a**, and **25a**[13] (see Supporting Information for individual structures) provide insight into why this might be (Figure 8).

Table 2. Synthesis of 8·Pd(Ar)Br Complexes

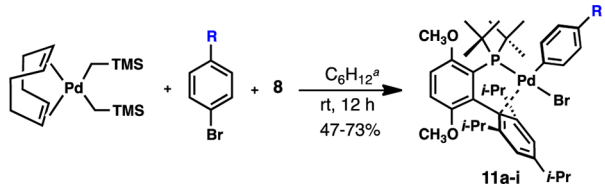

entry	R	yield[b] (%)	entry	R	yield[b] (%)
18a	$N(CH_3)_2$	57	**22a**	F	47
19a	OCH_3	52	**23a**	Cl	73
11a	*n*-Bu	59[c]	**24a**	CHO	67
20a	H	66	**25a**	CN	66[d]
21a	Ph	73			

[a]Reaction conditions: 1.0 equiv of (1,5-cyclooctadiene)Pd-$(CH_2TMS)_2$, 1.0 equiv of **8**, 1.1−5.0 equiv of aryl bromide, cyclohexane, 12 h. [b]Isolated yields, not optimized. [c]Reference 15. [d]Reference 13.

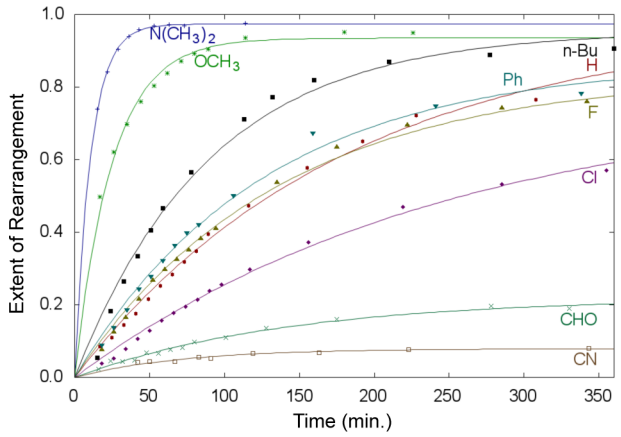

Figure 6. Growth of dearomatized product in the rearrangement of various **8**·Pd(Ar)Br complexes. A first-order kinetic model is overlaid for each.

No significant changes in the length of Pd−Br (2.46−2.47 Å) and Pd−P (2.34−2.35 Å) bond lengths were found among the four complexes, and the expected changes in the Ar−Pd−Br bond angles based on the relative ease of reductive elimination were observed.[28] The Pd−C1′ (*ipso* carbon of the lower ring) distance grows longer as the aryl group becomes more electron-rich (see Figure 9), due to the stronger *trans* influence of electron-rich aryl ligands. Likewise, the Pd−Ar bond lengthens slightly as the aryl substituent becomes more electron-rich, likely due to the weaker π-accepting ability of more electron-rich aryl substituents. Therefore, increasing the electron-donating ability of the aryl group weakens stabilization of the oxidative addition complex by the lower ring, making oxidative addition complexes with electron-rich aryl substituents less stable than those with electron-withdrawing aryl substituents. This effect could also facilitate the proposed *cis*/*trans* isomerization step in Pathways I and II if lower-ring disassociation is necessary for this process to occur.

Although the Hammett plot of the rates of isomerization (k_{f+r}) in Table 3 was nonlinear (not shown), the Hammett plot of the k_f values was linear, yielding $\rho = -1.58 \pm 0.16$ (Figure 9),[27] confirming that electron-donating groups on the aryl substituent increase the rate of dearomatization. This is likely due in part to the aforementioned ground-state weakening of

dx.doi.org/10.1021/ja310351e | J. Am. Chem. Soc. 2012, 134, 19922−19934

Table 3. Aryl Substituent Effects on Rearrangement: Thermodynamic and Kinetic Parameters

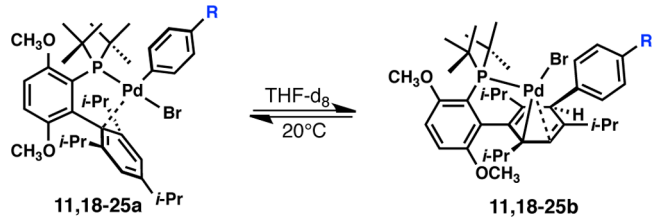

entry		R	σ	thermodynamic K_{eq}	thermodynamic ΔG_{exp} (kcal/mol)	kinetic k_{f+r}[c]	kinetic k_f[c]
18a	**18b**	$N(CH_3)_2$	−0.83	(40.5)[a]	(−2.2)[a]	>10	>11
19a	**19b**	OCH_3	−0.27	19.4 ± 0.34	−1.73 ± 0.01	3.35 ± 0.13	3.93 ± 0.14
11a	**11b**	*n*-Bu	−0.16	8.71 ± 0.15	−1.26 ± 0.01	1.50 ± 0.05	1.66 ± 0.06
20a	**20b**	H	0.00	4.32 ± 0.08	−0.85 ± 0.01	1.00 ± 0.03	1.00 ± 0.04
21a	**21b**	Ph	0.01	3.24 ± 0.06	−0.68 ± 0.01	1.02 ± 0.04	0.96 ± 0.03
22a	**22b**	F	0.06	3.61 ± 0.06	−0.75 ± 0.01	1.01 ± 0.05	0.97 ± 0.03
23a	**23b**	Cl	0.23	1.48 ± 0.03	−0.23 ± 0.01	0.86 ± 0.04	0.63 ± 0.02
24a	**24b**	CHO	0.42	0.24[b]	0.83 ± 0.01	0.99 ± 0.05	0.24 ± 0.01
25a	**25b**	CN	0.66	0.09[b]	1.43 ± 0.01	–[d]	–[d]

[a]From a first-order kinetic model. [b]Estimated error is less than ±0.01. [c]Relative to **20a** in THF-d_8. [d]Kinetics unreliable.

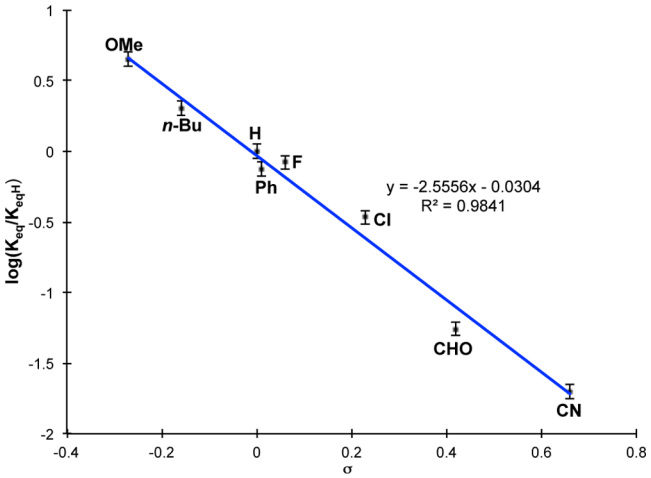

Figure 7. Hammett plot of equilibrium constants for the rearrangement of **8**·Pd(Ar)Br complexes (Table 3).[28]

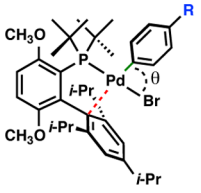

R	θ (°)	Pd-*ipso* (Å)	Pd-Ar (Å)
n-Bu (**11a**)	81.(3)	2.50(4)	2.01(6)
H (**20a**)	80.(0)	2.50(0)	2.01(4)
F (**22a**)	80.(0)	2.47(0)	2.01(2)
CN (**25a**)	79.(8)	2.45(2)	2.00(0)

Figure 8. Pd−Ar and Pd−*ipso* bond lengths, and Ar−Pd−Br bond angles for **11a**, **20a**, **22a**, and **25a**, derived from X-ray crystallographic analysis.

the Pd−C_{Ar} and Pd−C1′ bonds as the aryl substituent becomes more electron-rich, as these bonds must be cleaved for the insertion to occur. In addition, in the transition state of a concerted insertion C_{Ar} migrates from Pd to C2′, which is more electronegative than Pd, and thus C_{Ar} would be expected to become more electron-deficient as the insertion occurs. Electron-donating groups on the aryl substituent would mitigate this loss in electron density and thus facilitate the proposed concerted rearrangement. Therefore, the Hammett

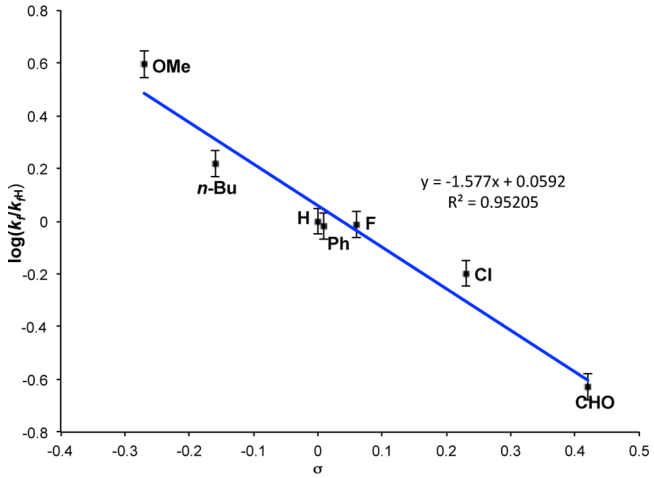

Figure 9. Hammett plot of the forward rate constants (k_f) for the rearrangement of **8**·Pd(Ar)Br complexes (Table 3).

plot in Figure 9 is also consistent with a concerted insertion process.

2.4. Halide Effect. We next investigated the influence of the halide ligand on the rearrangement of *t*BuBrettPhos oxidative addition complexes. The chloride (**26a**), iodide (**27a**), and triflate (**28a**) analogues of **11a** were prepared in the same manner as **11a** (Table 4). Pd(II) complexes bearing Cl, Br, and I ligands all feature ^{31}P NMR resonances in the δ 65−70 ppm range (CD_2Cl_2); however, triflate complex **28a** possesses a much further downfield ^{31}P resonance (δ 111 ppm, C_6D_6), suggesting the triflate group is dissociated in solution. X-ray crystallographic analysis revealed that the phenyl analogue of **28a** is formally cationic at Pd in the solid state, with additional stabilization provided by the lower ring of the ligand (Figure 10). Not surprisingly, **28a** was found to be susceptible to solvent coordination, so its rearrangement to **28b** was studied in C_6D_6 instead of THF-d_8. Iodide complex **27a** proved unstable in both THF-d_8 and C_6D_6, with free ligand slowly growing in (with generation of Pd black), in addition to a species with ^{31}P NMR (121 MHz, C_6D_6) shift at approximately

dx.doi.org/10.1021/ja310351e | J. Am. Chem. Soc. 2012, 134, 19922−19934

Table 4. Halide Effects on Rearrangement

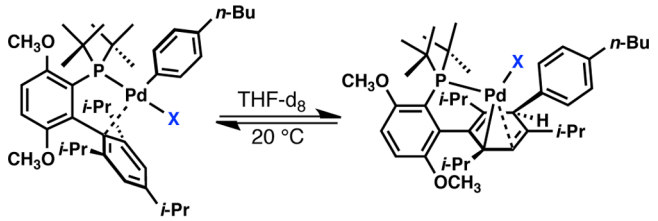

26a: X = Cl (73%)[a]
11a: X = Br (59%)[15]
27a: X = I[b] (53%)[a]
28a: X = OTf (37%)[a]

26b: X = Cl
11b: X = Br
27b: X = I
28b: X = OTf

entry		k_{f+r}[c]	k_f[c]	K_{eq}	ΔG_{exp} (kcal/mol)
26a	**26b**	2.84 ± 0.08	2.18 ± 0.07	2.15 ± 0.04	−0.44 ± 0.01
11a	**11b**	1.00 ± 0.03	1.00 ± 0.03	8.71 ± 0.15	−1.26 ± 0.01
28a	**28b**	–[d]	–[d]	0.04[e]	1.87 ± 0.01

[a]Isolated yield, prepared in the same manner as in Table 2. [b]Decomposed in solution. [c]Relative to **11a** in THF-d_8. [d]Kinetics unreliable due to small change in [**28a**] over time. [e]Value in C_6D_6; estimated error is less than ±0.01.

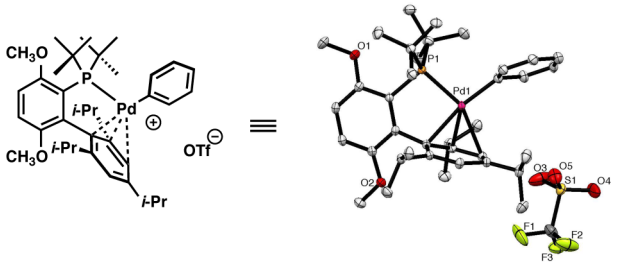

Figure 10. Solid-state structure of **8**·Pd(Ph)OTf. Ellipsoids shown at 50% probability.

δ 120 ppm.[29] Thus, we hesitate to assign definite kinetic or thermodynamic parameters to its rearrangement to **27b**. The observed trend for equilibrium constants is Br > Cl ≫ OTf (Table 4), which follows the trend observed in Table 3, as Cl is inductively more electron-withdrawing than Br, and the OTf complex **28a** is formally cationic. Although **27a** eventually decomposed in solution, we observed minimal formation of **27b** (~16%) during the first hour in THF-d_8, consistent with a rate trend of Cl > Br > I.

Exchanging the bromide ligand in **11a** for a chloride ligand in **26a** accelerates the rate of rearrangement (as with an electron-donating aryl substituent, Figure 9) but reduces the extent of rearrangement (as with an electon-withdrawing aryl substituent, Figure 7). Although Cl is inductively more electron-withdrawing than Br, it is a stronger π-donor to the Pd center; thus, the interplay of these two effects likely causes the observed difference in reactivity between **11a** and **26a**. However, at this time we cannot determine what role the halide ligand has in the rearrangement process.

2.5. Ligand Structure Effects. *2.5.1. Groups on Phosphorus.* The alkyl groups bound to phosphorus in biaryl phosphine ligands play a key role in determining the catalytic activity of their Pd complexes; bulkier ligands, i.e., those bearing *tert*-butyl and adamantyl groups, are typically used in cross-coupling reactions that have difficult reductive elimination steps. Thus, we decided to investigate the behavior of complexes of ligands analogous to **8** with different substituents on the phosphorus atom. Several oxidative addition complexes of the dicyclohexyl ligand BrettPhos (**7**) have been previously reported.[4,11,30] In none of these reports was any rearrangement of the corresponding oxidative addition complexes observed, although complexes derived from BrettPhos were found to exist as either C- or O-bound isomers is solution (these isomers are not observed in complexes of di-*tert*-butyl ligands). Considering Doyle's recent observation of **15**,[16] we decided to monitor the solution stability of **7**·Pd(4-*n*-BuPh)Br (**29a**)[4] by ^{1}H NMR (Table 5). Even after 10 days in solution no rearrangement to **29b** was observed. Oxidative addition complexes of other dicyclohexyl based biaryl phosphine ligands, including **2**,[1b,31]

Table 5. Phosphine Substituent Effects on Rearrangement

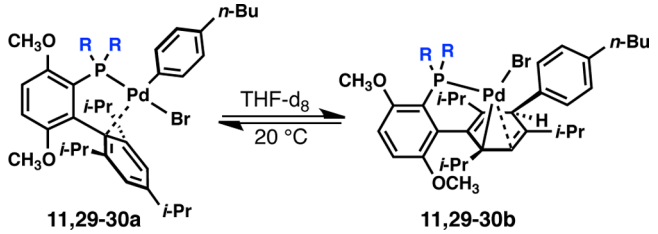

11,29-30a **11,29-30b**

entry		R	yield[a] (%)	k_{f+r}[b]	k_f[b]	K_{eq}	ΔG_{exp} (kcal/mol)
29a	**29b**	Cy	72	–	–	–[c]	–
11a	**11b**	*t*-Bu	37	1.00 ± 0.03	1.00 ± 0.03	8.71 ± 0.15	−1.26 ± 0.01
30a	**30b**	Ad	59	0.87 ± 0.04	0.87 ± 0.03	9.00 ± 0.16	−1.28 ± 0.01

[a]Isolated yield, prepared in the same manner as in Table 2. [b]Relative to **11a** in THF-d_8. [c]Rearranged product not observed. Ad = adamantyl.

dx.doi.org/10.1021/ja310351e | J. Am. Chem. Soc. 2012, 134, 19922−19934

Table 6. Ligand Substituent Effects on Rearrangement

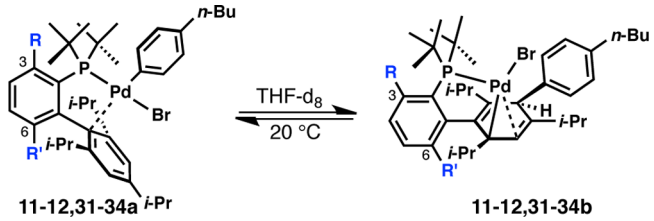

11-12,31-34a 11-12,31-34b

entry		R	R′	yield[a] (%)	k_{f+r}[b]	k_f[b]	K_{eq}	ΔG_{exp} (kcal/mol)
11a	**11b**	OMe	OMe	59	1.00 ± 0.03	1.00 ± 0.03	8.71 ± 0.15	−1.26 ± 0.01
12a	**12b**	OMb	Me	76	–[c]	–[c]	0.19[d]	0.97 ± 0.01
31a	**31b**	H	H	77	3.77 ± 0.54	0.87 ± 0.07	0.26[d]	0.78 ± 0.01
32a	**32b**	OMe	H	58	–[e]	–[e]	10.0 ± 0.2	−1.34 ± 0.01
33a	**33b**	Me	H	35	–[e]	–[e]	15.0 ± 0.3	−1.58 ± 0.01
34a	**34b**	H	Me	34	–[c]	–[c]	0.01[d]	2.68 ± 0.01

[a]Isolated yields; prepared in the same manner as in Table 2. [b]Relative to **11a** in THF-d_8. [c]Kinetics unreliable. [d]Estimated error is less than ±0.01. [e]Obtained at equilibrium.

3,[30] and **4**,[1b] have also been prepared or detected *in situ* with no report of anomalous behavior. To further test the effect of the substituents on phosphorus, **30a** was synthesized using the recently reported di-adamantyl analogue of **8**.[13] In solution, this complex rearranges to **30b** with kinetic and thermodynamic parameters similar to those observed for the conversion of **11a** to **11b** (Table 5). This is not surprising, given the similar size of the *tert*-butyl and adamantyl groups near the Pd center. Thus, the relief of unfavorable steric interactions between the aryl group and *tert*-butyl (or adamantyl) groups is likely a driving force for rearrangement, as it is for reductive elimination. This finding is consistent with the positive $\Delta S^{\ddagger}$ of the rearrangement process (*vide supra*), as the rearranged species should possess more rotational degrees of freedom for both the *tert*-butyl and aryl substituents than in the corresponding oxidative addition complex.

2.5.2. Substituents on the Biaryl Backbone. Due to the radically different behavior of complexes of *t*BuBrettPhos (**8**) and RockPhos (**10**), the effect of substituents on the phosphine-containing ring of the biaryl backbone was investigated. Because a change from a methoxy group in the 6-position of **11a** to a methyl group in **12a** greatly decreased the K_{eq} and rate of rearrangement (~5% rearrangement after 6 h), we hypothesized that bulkier substituents in the in the 6-position might retard rearrangement. Similarly, the fact that **5**·Pd(4-*n*-BuPh)Br (**31a**) was found to rearrange to **31b** to only a small degree (Table 6) suggested that the substituent in the 3-position found in **11a** but not in **31a** might promote rearrangement. Thus, a variety of complexes were synthesized in order to test the effect of substituents in the 3- and 6-positions on the rate of rearrangement and the equilibrium ratio of complexes (Table 6). When attempting to prepare **32a**, the oxidative addition complex of a BrettPhos-type ligand with no substituent in the 6-position,[3b] we observed that the product that precipitated from the reaction mixture was already an equilibrium mixture heavily favoring rearranged complex **32b** (Table 6). To probe whether the enhancement of rearrangement by a substituent in the 3-position was due to either steric or electronic effects, we attempted to synthesize **33a** (R = Me).[32] As with **32a**, only an equilibrium mixture favoring **33b** could be obtained (Table 6). An equilibrium constant (K_{eq}) of 15 was determined for this complex and is the largest value seen for any ligand in the series of oxidative addition complexes where Ar = 4-*n*-BuPh. Finally, **34a**, which has a methyl group in the 6-position but no substituent in the 3-position of the ligand, was prepared. In accordance with previous findings, only trace amounts (~1%) of **34b** could be detected in solution by ^{1}H NMR.

Overall, these results confirm that substituents in the 3-position promote both the rate and extent of dearomatization, whereas substituents in the 6-position inhibit the process. Based on the equilibrium constants of complexes **32a**/**32b** and **33a**/**33b**, the promotion of rearrangement by substituents at the 3-position appears to be a steric effect that most likely arises from this substituent "pushing" the *tert*-butyl groups closer to the Pd center, an effect also thought to promote reductive elimination. The solid-state structures of **11a**, **12a**, and **11b** provide an explanation for the effect of substituents in the 6-position of the phosphine-containing ring on the extent of rearrangement at equilibrium. Viewing **11a** and **12a** along the axis that contains the biaryl bond and bisects both the lower and phosphine-containing rings (as shown in Figure 11), the lower and phosphine-containing rings are almost perfectly perpendicular to one another, as would be expected. Due to the near perpendicularity of the two rings, the distance between the *ortho*-isopropyl groups and the substituent at the 6-position (a methoxy group in **11a**, a methyl group in **12a**) is similar, with an observed average distance of 3.55 Å in **11a** and 3.77 Å in **12a**. The longer observed distance in **12a** than in **11a** reflects the longer bond length of the C−C bond in **12a** (1.51(4) Å) compared to the C−O bond in **11a** (1.37(6) Å).

However, viewing the solid-state structure of **11b** in the same manner reveals that the lower ring is significantly tilted relative to the phosphine-containing ring following dearomatization (Figure 12). This tilting effectively positions the isopropyl group adjacent to the Pd-center farther from the methoxy goup at the 6-position but, more importantly, positions the other isopropyl group (highlighted in yellow in Figure 12) roughly 0.56 Å closer to the methoxy group than it was in **11a**. The decrease in distance between these two substituents upon dearomatization should result in a stronger steric interaction between them. In **12b** the substituent at the 6-position is a significantly larger than that in **11a**, suggesting that the increase in steric repulsion following dearomatization should be even more dramatic for **12b** than for **11b** and could be enough to significantly destabilize the dearomatized complex. This

dx.doi.org/10.1021/ja310351e | J. Am. Chem. Soc. 2012, 134, 19922−19934

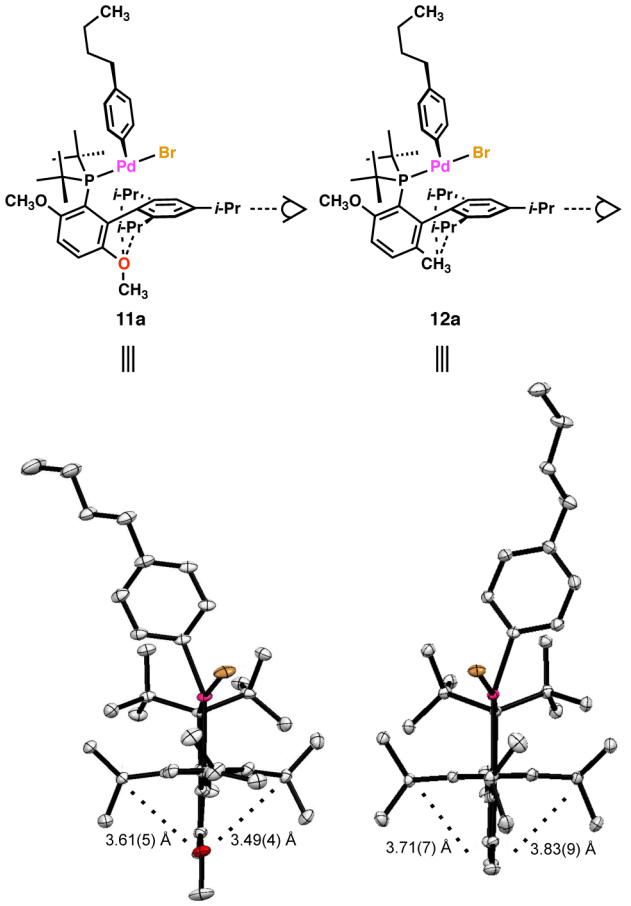

Figure 11. Intramolecular distances between the 6-substituent and the *ortho*-isopropyl group in **11a** (left) and **11b** (right). Ellipsoids shown at 50% probability.

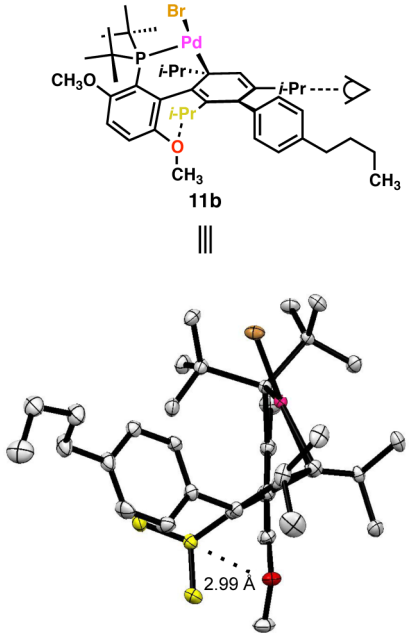

Figure 12. Intramolecular distance between the 6-methoxy group and one of the *ortho*-isopropyl groups on the lower ring of the ligand in **11b**. Ellipsoids shown at 50% probability.

ground-state effect is the most likely explanation for why **12a** dearomatizes to such a lesser extent than **11a**. The effect of the substituent at the 6-position on transition states, and thus its effect on the relative rates of rearrangement for the two complexes, is more difficult to determine.

2.5.3. Further Studies of Complexes of 5 and 10. In order to determine if the trends we observed for complexes of **8** were generalizable to other commonly employed di-*tert*-butyl biaryl phosphine ligands, we further examined the reactivity of complexes bearing *t*BuXPhos (**5**) and RockPhos (**10**) as ligands. Thus, additional complexes of **5** (**35a**–**38a**) and **10** (**38**–**40a**) were synthesized to compare with the corresponding complexes of **8** (Tables 7 and 8). Crystal structures of these

Table 7. Equilibrium Parameters for the Rearrangement of Various Aryl-Substituted Complexes Derived from 5

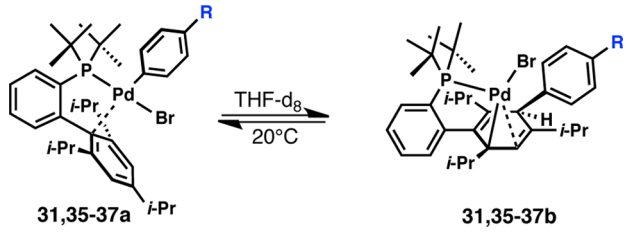

a	b	R	yield[a] (%)	K_{eq}	ΔG_{exp} (kcal/mol)
35a	**35b**	$N(CH_3)_2$	77	2.15 ± 0.04	−0.45 ± 0.01
31a	**31b**	*n*-Bu	77	0.26[b]	0.78 ± 0.01
36a	**38b**	H	70	0.11[b]	1.28 ± 0.01
37a	**37b**	CN	67	–[c]	–[c]

[a]Isolated yields; prepared in analogy to Table 2. [b]Estimated error is <0.01. [c]Rearranged species not detected by ^{1}H NMR.

Table 8. Equilibrium Parameters for the Rearrangement of Various Aryl-Substituted Complexes Derived from 10

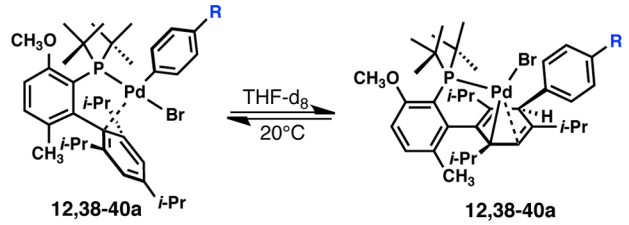

a	b	R	yield[a] (%)	K_{eq}	ΔG_{exp} (kcal/mol)
38a	**38b**	$N(CH_3)_2$	75	1.08 ± 0.02	−0.05 ± 0.01
12a	**12b**	*n*-Bu	76[b]	0.19[c]	0.97 ± 0.01
39a	**39b**	H	76	0.08[c]	1.47 ± 0.01
40a	**40b**	CN	70	–[d]	–[d]

[a]Isolated yields; prepared in analogy to Table 2. [b]Reference 15. [c]Estimated error is <0.01. [d]Rearranged species not detected by ^{1}H NMR.

complexes were obtained and show similar structural features and trends to those of **8**, including the lengthening of the Pd–*ipso* interaction as the arene becomes more electron-rich (see Supporting Information for individual X-ray structures). The aryl substituent equilibrium constant trend of NMe_2 > *n*-Bu > H > CN demonstrated for complexes of **8** in Table 3 was also observed for complexes of **5** and **10**, with no detectable rearrangement of **37a** and **40a** observed even after several days in solution (Tables 7 and 8). In addition, the observed trend in extent of rearrangement for varying the phosphine ligand in the

dx.doi.org/10.1021/ja310351e | J. Am. Chem. Soc. 2012, 134, 19922–19934

4-*n*-BuPh complex series, namely **8** > **5** > **10** (Table 6), also held true for the 4-NMe_2 and Ph series. Thus, the results and analysis we described for complexes of **8** likely hold true for complexes of **5** and **10** as well.

Taken together, these results show that the rearrangement of dialkyl biaryl phosphine-ligated Pd(II) complexes is heavily dependent on the steric parameters of both the phosphine-containing ring of the ligand and well as the alkyl groups on the phosphorus atom.[33] It is important to note that all studied complexes bearing di-*tert*-butyl biaryl phosphine ligands show at least some ability to rearrange in solution except for the arylated *t*BuBrettPhos complex **13**. Interestingly, the main structural difference between **11a** and **13** is a distortion from ideal square-planar geometry observed in **11a** (and in all solid-state structures that have been obtained for oxidative addition complexes of **5**, **8**, and **10**) that is not observed in the solid-state structure of **13**.[34] When **11a** is viewed down the biaryl axis (as shown in Figure 11), it becomes clear that the angle between the *ipso* carbon and the aryl substituent (*ipso*–Pd–Ar) is not 180° as it would be in an ideal square planar complex; instead, this angle is approximately 158° due to tilting of the aryl substituent toward one side of the lower ring of the ligand. In addition, the P–Pd–Br angle is distorted approximately 13° from linearity. This "tilting" could indicate a ground-state predilection toward dearomatization in these complexes. However, when **13** is viewed in the same manner (as shown in Figure 13), no significant distortion of the *ipso*–Pd–Ar angle

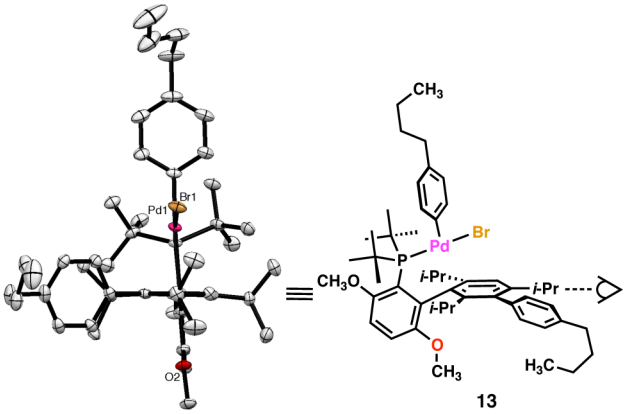

Figure 13. Solid-state structure of **13**, showing no significant distortions of the *ipso*–Pd–Ar and P–Pd–Br angles from linearity and containing a more ideal square planar geometry than **11a** (Figure 11).

(178° in **13**) from linearity is observed, and the P–Pd–Br is significantly closer to linearity (176°) than in **11a**. Thus, the 3′-aryl substituent imposes a stronger square planar geometry at the metal center, which seems to prevent a second dearomatization event from occurring.

3. COMPUTATIONAL STUDIES

3.1. Calibration of Structures and Energies for 11a and 11b. In order to shed more light on the rearrangement process, especially with regard to the mechanism of aryl insertion, we turned to density functional theory (DFT). All calculations were performed using the Q-Chem quantum chemistry package.[35] Density functionals and basis sets were evaluated based on their ability to reproduce the experimentally determined relative energies of **11a** and **11b**, as well as the structural features present in both solid-state structures. The basis set LANL2DZ[36,37] was used for all calculations. The Perdew–Becke–Ernzerhof (PBE) functional[38] resulted in the most accurate energy difference between **11a** and **11b** (ΔE = −0.43 kcal/mol); most other tested density functionals gave ΔE values that were too large (see Supporting Information).[39] In addition, the optimized geometry of **11a** using PBE/LANL2DZ was found to closely resemble the obtained crystal structure. For example, whereas other functionals overestimated the length of the *ipso* interaction, indicating an incorrect treatment of this unusual bonding mode, PBE/LANL2DZ reproduced this distance fairly accurately (calc 2.58 Å, expt 2.53 Å). The optimized structures of **11a** and **11b** using PBE/LANL2DZ are shown in Figure 14; this basis set and density

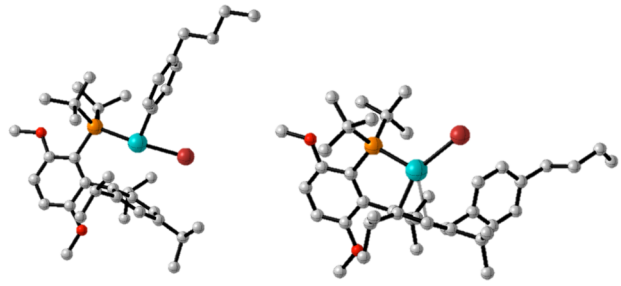

Figure 14. Optimized geometries of **11a** (left) and **11b** (right) using PBE/LANL2DZ.

functional combination were chosen for all subsequent computational work. The choice of PBE/LANL2DZ was further validated by the ability of this basis set/functional combination to reproduce the experimental trend for the relative energies of the series of aryl-substituted oxidative addition complexes of **8** shown in Table 3 (Table 9). Notably, the DFT calculations systematically underestimate how much of the rearranged isomer should be present at equilibrium. A Hammett plot of the calculated equilibrium constants (Figure 15) shows a worse linear fit than the experimental data (due primarily to the outlier CHO data point), but yielded ρ = −2.78

Table 9. Experimental ΔG and Calculated ΔE Values for Various 8·Pd(Ar)Br Complexes

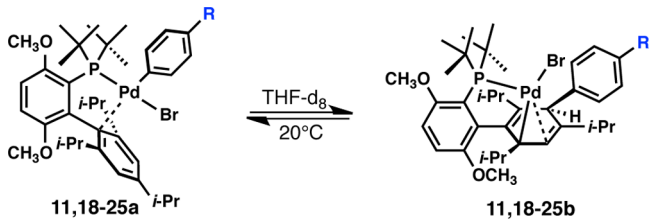

a	b	R	σ	ΔG_{exp} (kcal/mol)[a]	ΔE (kcal/mol)
18a	**18b**	$N(CH_3)_2$	−0.83	(−2.2)[b]	−2.28
19a	**19b**	OCH_3	−0.27	−1.73 ± 0.01	−1.35
11a	**11b**	*n*-Bu	−0.16	−1.26 ± 0.01	−0.43
20a	**20b**	H	0.00	−0.85 ± 0.01	0.02
21a	**21b**	Ph	0.01	−0.6B ± 0.01	0.40
22a	**22b**	F	0.06	−0.75 ± 0.01	−0.03
23a	**23b**	Cl	0.23	−0.23 ± 0.01	1.17
24a	**24b**	CHO	0.42	0.83 ± 0.01	2.93
25a	**25b**	CN	0.66	1.43 ± 0.01	2.46

[a]In THF-d_8. [b]Estimated using a first-order kinetic model.

dx.doi.org/10.1021/ja310351e | J. Am. Chem. Soc. 2012, 134, 19922–19934

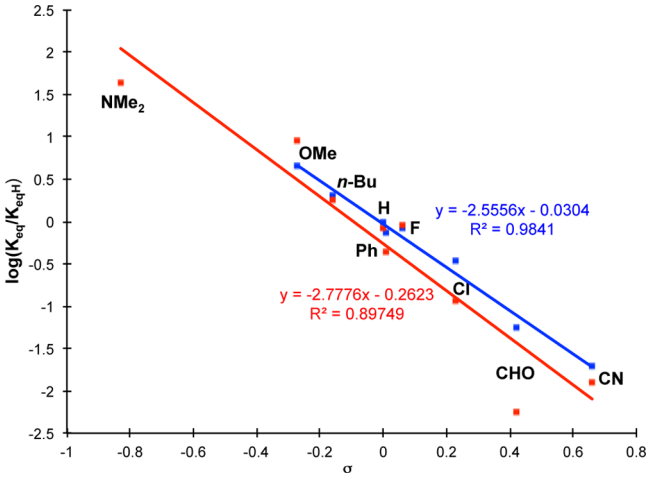

Figure 15. Theoretical (red) and experimental (blue) Hammett plot for the rearrangement of **8**·Pd(Ar)Br complexes.

± 0.36, which agrees well with the experimentally determined ρ value of −2.56 ± 0.13 (Figure 7).[40] Thus, the PBE/LANL2DZ combination adequately reproduces the structural trends observed for complexes of **8**.

3.2. Molecular Orbital Description of Rearrangement. The optimized geometry and solid-state structure of **11b** both possess a trigonal planar geometry around the Pd(II) center, distinct from the more commonly observed square planar geometry assumed by **11a**. By comparing the relative ordering of the 4d orbitals in the Kohn−Sham molecular orbitals (MOs) obtained from DFT calculations for **11a** and **11b** (see Computational Supporting Information for all calculated MOs), we can establish the extent of crystal field splitting for these two complexes. Thus, the relative 4d orbital ordering of $xz < xy < yz < z^2 < x^2-y^2$ for **11a** and $xz < xy < z^2 < yz < x^2-y^2$ for **11b** dictates that both complexes reside in the regime of large crystal field splitting (see Supporting Information for more detailed calculations).[41,42] This is important because in this regime a trigonal planar geometry around a Pd(II) center can be close in energy to a square planar geometry. A strong ligand field for these complexes would also explain the weak effect of solvent on the rate and extent of rearrangement observed in Table 1, as the identity of the solvent should not significantly change the electronic environment of the metal center.

We further examined those Kohn−Sham MOs for **11a** and **11b** that show any orbital interaction between the 4d orbitals on the metal center and the lower ring of the ligand to investigate the *ipso* interaction in **11a** as well as the fate of this interaction after rearrangement to **11b**. Overlap between one lobe of Pd $4d_{yz}$ and the π-system of the lower ring (σ1, Figure 16) at C1′ suggests that the *ipso* interaction is analogous to a

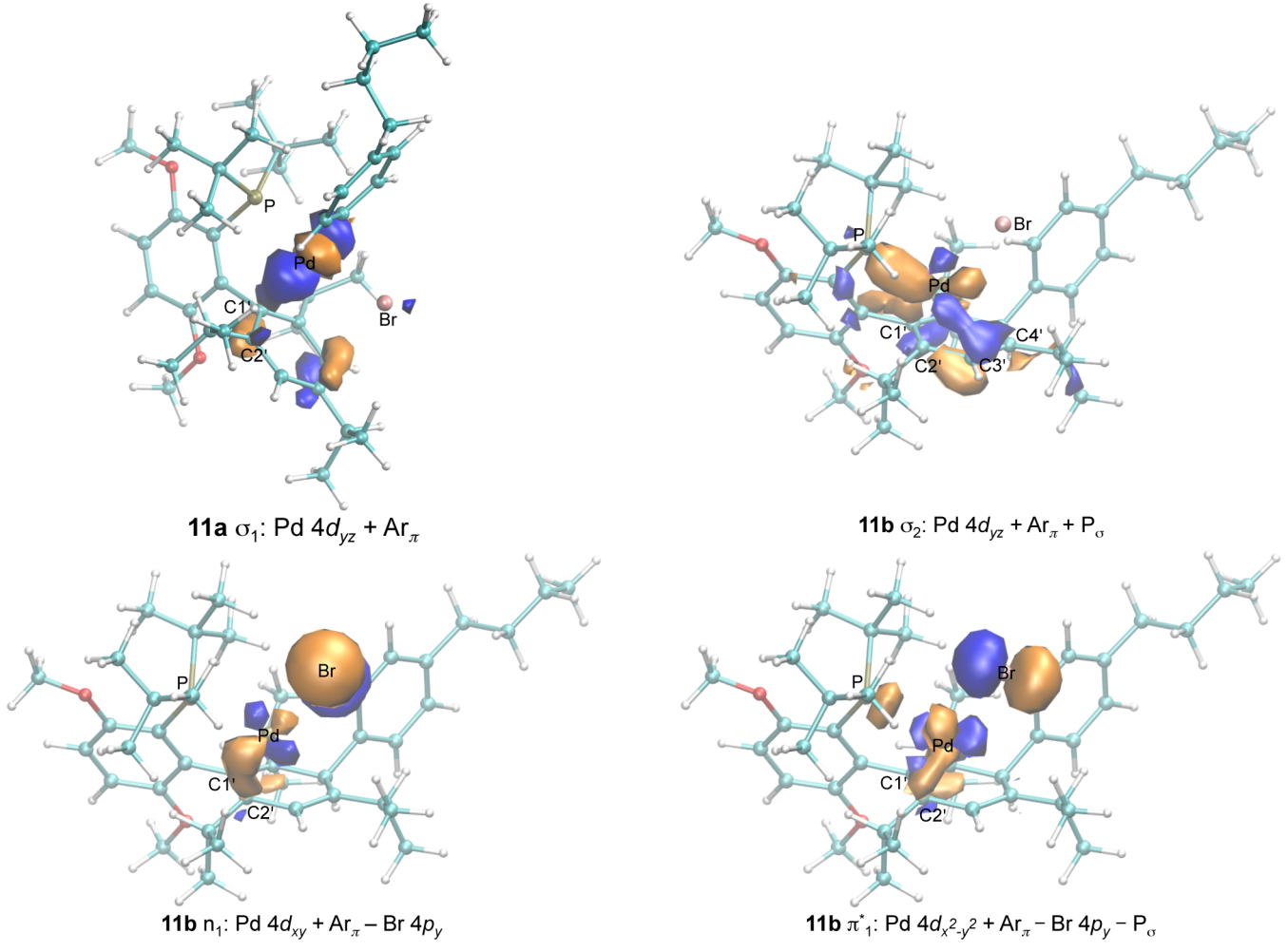

Figure 16. Selected Kohn−Sham molecular orbitals for **11a** (σ_1) and **11b** (σ_2, n_1, π^*_1).

dx.doi.org/10.1021/ja310351e | J. Am. Chem. Soc. 2012, 134, 19922−19934

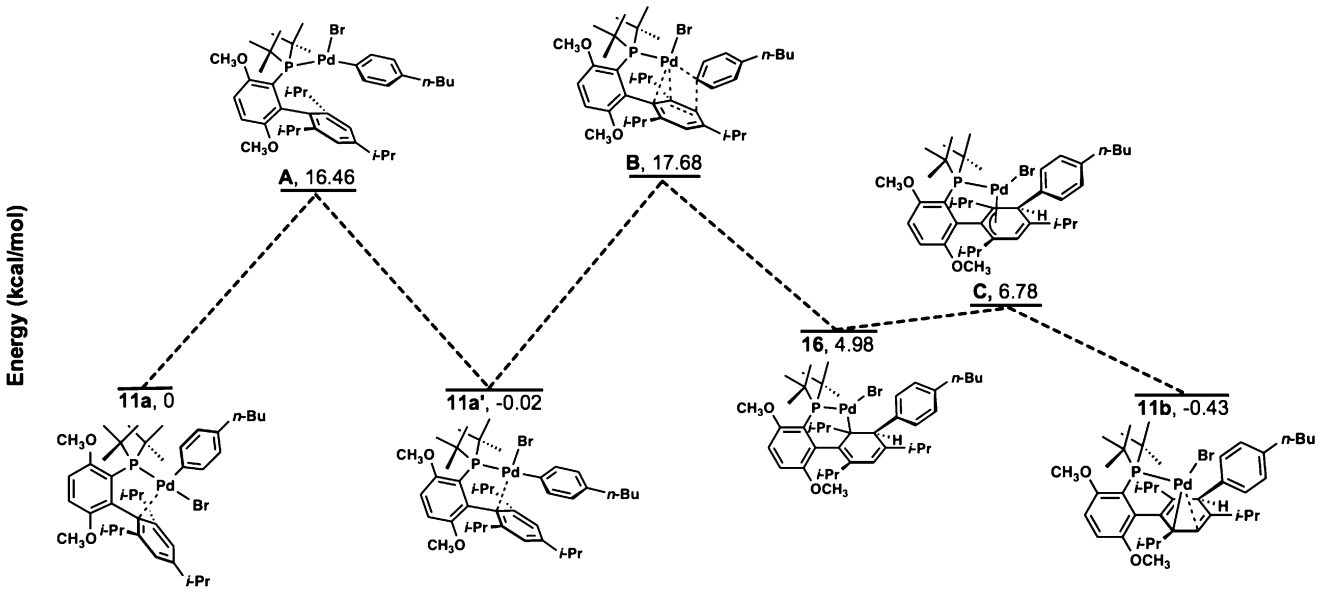

Figure 17. Calculated gas-phase reaction coordinate from **11a** to **11b**.

strong σ-bond between the lower ring and the Pd center. Interestingly, in this MO there is also a small amount of in-phase orbital density on adjacent C2′, which is where the Pd center ultimately forms a σ-bond during the dearomatization process. Thus, the dearomatization likely occurs by increasing this bonding interaction between the Pd-center and C2′ at the expense of the π-system of the lower ring.

Three relevant occupied MOs that depict the unusual bonding orientation in **11b** were also found (Figure 16); their relative energies are $\pi^*_1 > n_1 > \sigma_2$. In σ_2, the $4d_{yz}$ orbital, which in **11a** was overlapping with the π-system at C1′, now shows significant overlap with the π-bond between C3′ and C4′ (localized primarily at C3′). This strong interaction results in a short intramolecular distance (2.29(7) Å) between these two centers, and thus is likely stronger than the *ipso* interaction found in **11a**. There is also in-phase overlap between another lobe of $4d_{yz}$ and the π-bond at C1′ in this MO, suggesting that the original *ipso* interaction is still present in **11b** (albeit to a lesser degree than in **11a**). The MOs n_1 and π^*_1 are relevant because they show strong σ-type overlaps between 4d orbitals on the metal center and C2′, where a σ-bond has now formed (Figure 16). Together, these MOs reveal that the orbital overlap responsible for the *ipso* interaction in **11a** may be important for enabling orbital overlap between C2′ and 4d orbitals on the metal center, which is ultimately necessary for the formation of the σ-bond found between these two atoms in **11b**.

3.3. Reaction Coordinate from 11a to 11b. A combination of transition state searches and intrinsic reaction coordinate (IRC) calculations lead to a continuous reaction pathway from **11a** to **11b** (Figure 17).[43] Transition state **B** was located on the reaction pathway from **11a** to **11b**; it shows a direct 1,2-insertion of the aryl substituent into the lower ring of the ligand taking place, instead of the 1,4-insertion necessary to proceed directly from **11a** to **11b** (see Supporting Information for calculated structures). Its energy relative to **11a** (ΔE = 17.7 kcal/mol) closely matches the $\Delta G^{\ddagger}$ found via Eyring analysis (17.3 ± 1.3 kcal/mol) for the rearrangement of **11a** to **11b**, supporting the involvement of **B** in the rearrangement pathway.

Checking the IRC of transition state **B** led to new local minima on either side of the reaction coordinate instead of connecting back to **11a** and **11b**. As expected, **16** was found as a minimum leading to **11b** and is the direct product of the 1,2-insertion depicted in **B** (Figure 17). **16** was calculated to be significantly higher in energy than **11b** (5.4 kcal/mol), presumably due to unfavorable steric interactions between the Pd center and the adjacent aryl substituent. Proceeding forward along the reaction coordinate yielded low-lying transition state **C** between **16** and **11b**, which depicts a simple 1,3-migration of the Pd-center via a π-allyl species (Figure 17). The small barrier (1.8 kcal/mol relative to **16**) suggests that conversion of **16** to thermodynamically favored **11b** should be incredibly facile and too rapid for detection of **16** by NMR. Indeed, we have never observed a second rearranged species in any rearrangement conducted to date. Thus, DFT calculations predict that the second half of Pathway I (Scheme 1) is the most likely pathway for the rearrangement of **11a** to **11b**. Following the IRC of **B** backward lead not to **11a** but to the rotameric complex **11a′** (Figure 17).

Surprisingly, **11a′** was calculated to have almost the same energy as **11a** (−0.02 kcal/mol); calculations of an analogous *cis*/*trans* isomerization using the SPhos complex **2**·Pd(Ph)Cl predicted the isomer corresponding to **11a′** to be 9.7 kcal/mol higher in energy than the isomer corresponding to **11a**,[31a] purportedly due to the trans influence of the phosphine ligand. Because **8** is a much larger ligand than **2**, the *cis*/*trans* isomerization might be more favorable in the present case because it relieves unfavorable steric strain between the *tert*-butyl groups and the aryl substituent, at the cost of increased interactions between the lower ring of the ligand and the aryl substituent. Transition state **A** was found on the IRC between **11a** and **11a′**, and it forms by disassociation of the lower ring of the ligand and pseudo-rotation around the Pd center. The calculated barrier for this pseudo-rotation (16.5 kcal/mol) is higher than expected given that multiple oxidative addition complexes are not observable by ^{31}P or ^{1}H NMR at room temperature. The energy of **A** is likely overestimated due to the neglect of entropic effects in the DFT calculations, as **A** is more flexible than other complexes along the reaction coordinate.

dx.doi.org/10.1021/ja310351e | J. Am. Chem. Soc. 2012, 134, 19922−19934

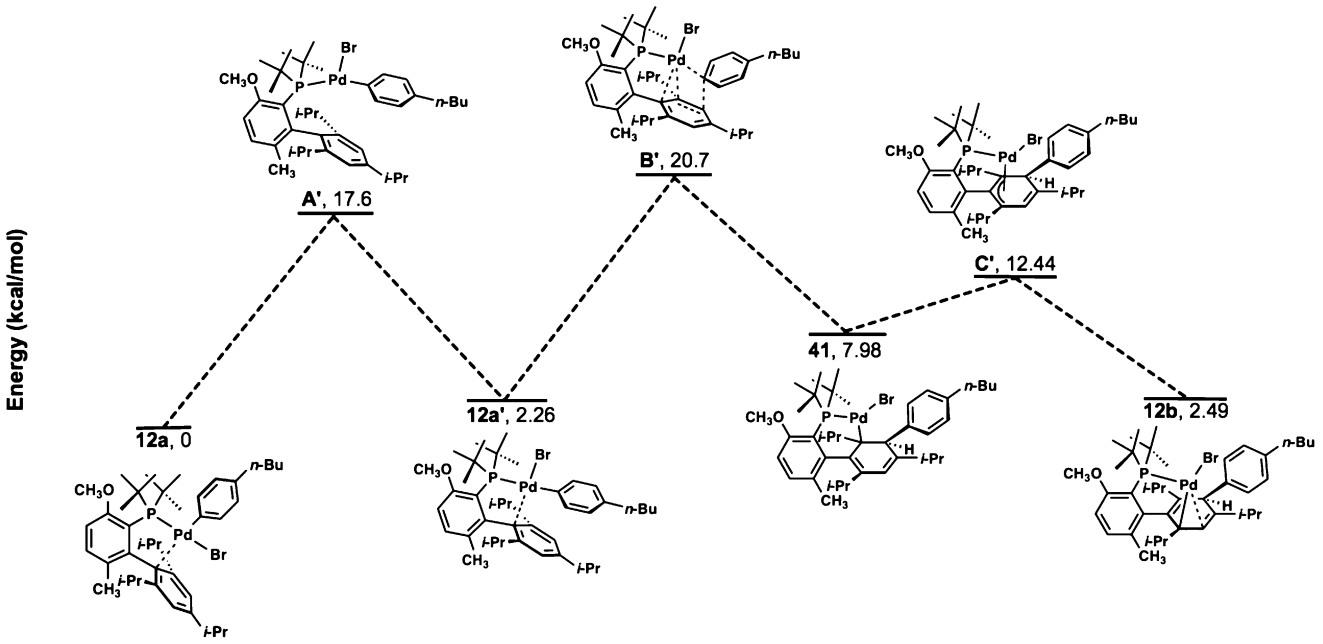

Figure 18. Calculated gas-phase reaction coordinate from **12a** to **12b**.

Solvent effects could also be crucial for stabilizing **A**. Nonetheless, the calculated reaction coordinate diagram supports a concerted mechanism for the insertion reaction under study, and suggests that Pathway I (Scheme 1) is operative during the rearrangement.

3.4. Reaction Coordinate from 12a to 12b. In order to gain further insight into the effect of ligand structure on the dearomatization reaction, we employed the same calculations used in Figure 17 to calculate the transition states leading from the analogous RockPhos-ligated complex **12a** to its rearranged isomer **12b**. The results of this analysis are shown in Figure 18.[44] DFT calculations predict **12a** to be lower in energy than **12b**, confirming that a substituent change in the 6-position of the phosphine-containing ring from OMe to Me is enough to destabilize the rearranged complex. A similar reaction pathway to that shown in Figure 17 was determined for the conversion of **12a** to **12b**: *cis*/*trans* isomerization via transition state **A′** to **12a′**, followed by 1,2-insertion via transition state **B′** to give **41**, and finally a 1,3-shift of the Pd center (via **C′**) to give **12b**. Transition states **A′**, **B′**, and **C′** are completely analogous to **A**, **B**, and **C** from Figure 17. The calculated barrier for the rate-determining insertion step is higher for **12a′** (20.7 kcal/mol) than for **11a′** (17.7 kcal/mol). However, the *cis*/*trans* isomerization barrier is calculated to be only slightly higher for **11a** compared with **11a**. Given the significantly broader ^{31}P resonance of **11a** compared to **12a** (Figure 5), one would expect this barrier to differ more substantially and this result may reflect the aforementioned inaccuracies in these gas-phase calculations pertaining to this step of the mechanism.[45] Nonetheless, DFT calculations suggest that the identity of the substituent in the 6-position of the phosphine-containing ring should have a significant impact on the rate and extent of rearrangement.

4. CONCLUSION

The presented computational and experimental work is consistent with a Pd(II)-mediated, direct aryl insertion reaction into an arene; until now, this reactivity had only been postulated as a potential pathway in some C−H arylation processes. We have found that not only is this process viable, but that it can occur under quite mild conditions in certain cases. The relief of unfavorable steric interactions between the alkyl groups on phosphorus and the aryl substituent is a powerful factor in promoting the rate and extent of rearrangement, as is the electronic nature of the aryl group. Taken together, these experimental and computational results suggest that the structural features that make bulky biaryl phosphine ligands such as **5**, **8**, and **10**, such effective ligands for promoting challenging reductive eliminations from Pd(II) also enable the rearrangement of their oxidative addition complexes to the corresponding dearomatized isomers. This knowledge should prove useful in the design of future ligands with improved catalytic activity and, ultimately, to bulky biaryl phosphine ligands that do not show signs of rearrangement or ligand arylation in catalytic processes.

■ ASSOCIATED CONTENT

Supporting Information

Procedural, spectroscopic, and X-ray crystallographic (CIF) data; kinetic graphs, including those used to determine relative rate constants; coordinates for all calculated complexes and other computational data; complete ref 35. This material is available free of charge via the Internet at http://pubs.acs.org.

■ AUTHOR INFORMATION

Corresponding Author

sbuchwal@mit.edu

Present Address

[†]Department of Chemistry, University of California, Berkeley, CA 94720

Notes

The authors declare the following competing financial interest(s): MIT has patents on ligands used during the course of this research, from which S.L.B. receives royalty payments.

■ ACKNOWLEDGMENTS

We thank the National Institutes of Health for financial support of this project (GM46059) and for a postdoctoral fellowship for T.J.M. (1F32GM088931). P.J.M. thanks the National Science Foundation for a pre-doctoral fellowship (2010094243) and an educational donation provided by Amgen, for which we are grateful. Dr. Alexander Duefert is acknowledged for providing the crystal structure of **21a**. J.C. thanks Prof. Troy Van Voorhis for helpful discussions and financial assistance. The Varian spectrometers used for portions of this work were purchased with funds from the National Science Foundation (Grants CHE 980861 and DBI 9729592). One of the X-ray diffractometers used was purchased with the help of funding from the National Science Foundation (Grant CHE 0946721). Michael Takase is acknowledged for solving several of the X-ray structures presented in this work.

■ REFERENCES

(1) For selected readings, see: (a) Martin, R.; Buchwald, S. L. *Acc. Chem. Res.* **2008**, *41*, 1461. (b) Kinzel, T.; Zhang, Y.; Buchwald, S. L. *J. Am. Chem. Soc.* **2010**, *132*, 14073. (c) Han, C.; Buchwald, S. L. *J. Am. Chem. Soc.* **2009**, *131*, 7532. (d) Martin, R.; Buchwald, S. L. *J. Am. Chem. Soc.* **2007**, *129*, 3844. (e) Martin, R.; Buchwald, S. L. *Org. Lett.* **2008**, *10*, 4561. (f) Martin, R.; Buchwald, S. L. *Angew. Chem., Int. Ed.* **2007**, *46*, 7236.

(2) Surry, D. S.; Buchwald, S. L. *Chem. Sci.* **2011**, *2*, 27.

(3) (a) Salvi, L.; Davis, N. R.; Ali, S. Z.; Buchwald, S. L. *Org. Lett.* **2012**, *14*, 170. (b) Wu, X.; Fors, B. P.; Buchwald, S. L. *Angew. Chem., Int. Ed.* **2011**, *50*, 9943. (c) Burgos, C. H.; Barder, T. E.; Huang, X.; Buchwald, S. L. *Angew. Chem., Int. Ed.* **2006**, *45*, 4321.

(4) Cho, E. J.; Senecal, T. D.; Kinzel, T.; Zhang, Y.; Watson, D. A.; Buchwald, S. L. *Science* **2010**, *328*, 1679.

(5) For C−F bond formation, see: (a) Watson, D. A.; Su, M.; Teverovskiy, G.; Zhang, Y.; García-Fortanet, J.; Kinzel, T.; Buchwald, S. L. *Science* **2009**, *325*, 1661. (b) Noel, T.; Maimone, T. J.; Buchwald, S. L. *Angew. Chem., Int. Ed.* **2011**, *50*, 8900. For C−X (X = Br, Cl) bond formation, see: (c) Pan, J.; Wang, X.; Zhang, Y.; Buchwald, S. L. *Org. Lett.* **2011**, *13*, 4974. (d) Shen, X.; Hyde, A. M.; Buchwald, S. L. *J. Am. Chem. Soc.* **2010**, *132*, 14076.

(6) Aranyos, A.; Old, D. W.; Kiyomori, A.; Wolfe, J. P.; Sadighi, J. P.; Buchwald, S. L. *J. Am. Chem. Soc.* **1999**, *121*, 4369.

(7) (a) Thaler, T.; Haag, B.; Gavryushin, A.; Schober, K.; Hartmann, E.; Gschwind, R. M.; Zipse, H.; Mayer, P.; Knochel, P. *Nat. Chem.* **2010**, *2*, 125. (b) Barder, T. E.; Walker, S. D.; Martinelli, J. R.; Buchwald, S. L. *J. Am. Chem. Soc.* **2005**, *127*, 4685.

(8) (a) Oberli, M. A.; Buchwald, S. L. *Org. Lett.* **2012**, *14*, 4606. (b) Cook, M.; McLaughlin, M. *Chem. Commun.* **2011**, *47*, 11104. (c) Tundel, R.; Ikawa, T.; Altman, R.; Buchwald, S. L. *Angew. Chem., Int. Ed.* **2006**, *45*, 6523. (d) Nguyen, H. N.; Huang, X.; Buchwald, S. L. *J. Am. Chem. Soc.* **2003**, *125*, 11818.

(9) (a) Stolley, R. M.; Guo, W.; Louie, J. *Org. Lett.* **2012**, *14*, 322. (b) Cho, E. J.; Buchwald, S. L. *Org. Lett.* **2011**, *13*, 6552. (c) Rosen, B. R.; Ruble, J. C.; Beauchamp, T. J.; Navarro, A. *Org. Lett.* **2011**, *13*, 2564. (d) Shekhar, S.; Dunn, T. B.; Kotecki, B. J.; Montavon, D. K.; Cullen, S. C. *J. Org. Chem.* **2011**, *76*, 4552. (e) Bhagwanth, S.; Waterson, A. G.; Adjabeng, G. M.; Hornberger, K. R. *J. Org. Chem.* **2009**, *74*, 4634. (f) Anderson, K. W.; Tundel, R. E.; Ikawa, T.; Altman, R. A.; Buchwald, S. L. *J. Am. Chem. Soc.* **2006**, *128*, 10694.

(10) (a) Ueda, S.; Su, M.; Buchwald, S. L. *J. Am. Chem. Soc.* **2012**, *134*, 700. (b) Ueda, S.; Su, M.; Buchwald, S. L. *Angew. Chem., Int. Ed.* **2011**, *50*, 8944.

(11) Fors, B. P.; Watson, D. A.; Biscoe, M. R.; Buchwald, S. L. *J. Am. Chem. Soc.* **2008**, *130*, 13552.

(12) (a) Vinogradova, E. V.; Fors, B. P.; Buchwald, S. L. *J. Am. Chem. Soc.* **2012**, *134*, 11132. (b) McGowan, M. A.; McAvoy, C. Z.; Buchwald, S. L. *Org. Lett.* **2012**, *14*, 3800. (c) Rosenberg, A. J.; Zhao, J.; Clark, D. A. *Org. Lett.* **2012**, *14*, 1764. (d) McGowan, M. A.; Henderson, J. A.; Buchwald, S. L. *Org. Lett.* **2012**, *14*, 1432. (e) Breitler, S.; Oldenhuis, N. J.; Fors, B. P.; Buchwald, S. L. *Org. Lett.* **2011**, *13*, 3262. (f) Dooleweerdt, K.; Fors, B. P.; Buchwald, S. L. *Org. Lett.* **2010**, *12*, 2350. (g) Maimone, T. J.; Buchwald, S. L. *J. Am. Chem. Soc.* **2010**, *132*, 9990. (h) Fors, B. P.; Buchwald, S. L. *J. Am. Chem. Soc.* **2009**, *131*, 12898. (i) Fors, B. P.; Dooleweerdt, K.; Zeng, Q.; Buchwald, S. L. *Tetrahedron* **2009**, *65*, 6576.

(13) Su, M.; Buchwald, S. L. *Angew. Chem., Int. Ed.* **2012**, *51*, 4710.

(14) (a) Pérez-Galán, P.; Delpont, N.; Herrero-Gómez, E.; Maseras, F.; Echavarren, A. M. *Chem. Eur. J.* **2010**, *16*, 5324. (b) Christmann, U.; Pantazis, D. A.; Benet-Buchholz, J.; McGrady, J. E.; Maseras, F.; Vilar, R. *J. Am. Chem. Soc.* **2006**, *128*, 6376. (c) Barder, T. E. *J. Am. Chem. Soc.* **2006**, *128*, 898. (d) Christmann, U.; Vilar, R.; White, A. J. P.; Williams, D. J. *Chem. Commun.* **2004**, 1294.

(15) Maimone, T. J.; Milner, P. J.; Kinzel, T.; Zhang, Y.; Takase, M. K.; Buchwald, S. L. *J. Am. Chem. Soc.* **2011**, *133*, 18106.

(16) Nielsen, D. K.; Doyle, A. G. *Angew. Chem., Int. Ed.* **2011**, *50*, 6056.

(17) Allgeier, A. M.; Shaw, B. J.; Hwang, T.-L.; Milne, J. E.; Tedrow, J. S.; Wilde, C. N. *Organometallics* **2012**, *31*, 519.

(18) For selected readings, see: (a) Pape, A. R.; Kaliappan, K. P.; Kündig, E. P. *Chem. Rev.* **2000**, *100*, 2917. (b) Chordia, M. D.; Harman, W. D. J. *Am. Chem. Soc* **2000**, *122*, 725. (c) Pearson, A. J. *Science* **1984**, *223*, 895.

(19) (a) Yin, B.; Cai, C.; Zeng, G.; Zhang, R.; Li, X.; Jiang, H. *Org. Lett.* **2012**, *14*, 1098. (b) Ariafard, A.; Tabatabaie, E. S.; Monfared, A. T.; Assar, S. H. A.; Hyland, C. J. T.; Yates, B. F. *Organometallics* **2012**, *31*, 1680. (c) Ren, Y.; Jia, J.; Zhang, T.-T.; Wu, H.-S.; Liu, W. *Organometallics* **2012**, *31*, 1168. (d) Zhang, S.; Wang, Y.; Feng, X.; Bao, M. *J. Am. Chem. Soc.* **2012**, *134*, 5492. (e) Rousseaux, S.; García-Fortanet, J.; Del Aguila Sanchez, M. A.; Buchwald, S. L. *J. Am. Chem. Soc.* **2011**, *133*, 9282. (f) Feller, M.; Ben-Ari, E.; Iron, M. A.; Diskin-Posner, Y.; Leitus, G.; Shimon; Konstantinovski, L.; Milstein, D. *Inorg. Chem.* **2010**, *49*, 1615. (g) García-Fortanet, J.; Kessler, F.; Buchwald, S. L. *J. Am. Chem. Soc.* **2009**, *131*, 6676. (h) Song, D.; Sliwowski, K.; Pang, J.; Wang, S. *Organometallics* **2002**, *21*, 4978. (i) Bao, M.; Nakamura, H.; Yamamoto, Y. *J. Am. Chem. Soc.* **2001**, *123*, 759.

(20) (a) Alberico, D.; Scott, M. E.; Lautens, M. *Chem. Rev.* **2007**, *107*, 174. (b) García-Cuadrado, D.; Braga, A. A. C.; Maseras, F.; Echaverren, A. M. *J. Am. Chem. Soc.* **2006**, *128*, 1066. (c) Lane, B. S.; Brown, M. A.; Sames, D. *J. Am. Chem. Soc.* **2005**, *127*, 8050. (d) Park, C.-H.; Ryabova, V.; Seregin, I. V.; Sromek, A. W.; Gevorgyan, V. *Org. Lett.* **2004**, *6*, 1159. (e) Glover, B.; Harvey, K. A.; Liu, B.; Sharp, M. J.; Tymoschenko, M. F. *Org. Lett.* **2003**, *5*, 301. (f) Hennessy, E. J.; Buchwald, S. L. *J. Am. Chem. Soc.* **2003**, *125*, 12084. (g) Toyota, M.; Ilangovan, A.; Okamoto, R.; Masaki, T.; Arakawa, M.; Ihara, M. *Org. Lett.* **2002**, *4*, 4293. (h) McClure, M. S.; Glover, B.; McSorley, E.; Millar, A.; Osterhout, M.; Roschangar, F. *Org. Lett.* **2001**, *3*, 1677.

(21) For processes involving a proposed β-aryl elimination from a Pd−alkoxide species, see: (a) Chtchemelinine, A.; Rosa, D.; Orellana, A. *J. Org. Chem.* **2011**, *76*, 9157. (b) Satoh, T.; Miura, M. *Top. Organomet. Chem.* **2005**, *14*, 1. (c) Terao, Y.; Wakui, H.; Nomoto, M.; Satoh, T.; Miura, M.; Nomura, M. *J. Org. Chem.* **2003**, *68*, 5236. (d) Terao, Y.; Wakui, H.; Satoh, T.; Miura, M.; Nomura, M. *J. Am. Chem. Soc.* **2001**, *123*, 10407. For a proposal of a similar β-aryl elimination/rearomatization process in a catalytic reaction, see: (e) Youn, S. W.; Kim, B. S.; Jagdale, A. R. *J. Am. Chem. Soc.* **2012**, *134*, 11308.

(22) β-Aryl elimination from isolated Rh(I) complexes has been demonstrated: (a) Zhao, P. J.; Incarvito, C. D.; Hartwig, J. F. *J. Am. Chem. Soc.* **2006**, *128*, 3124. (b) Zhao, P. J.; Hartwig, J. F. *J. Am. Chem. Soc.* **2005**, *127*, 11618.

(23) For selected readings, see: (a) Chen, O.; Lin, B.-L.; Fu, Y.; Liu, L.; Guo, Q.-X. *Res. Chem. Intermed.* **2005**, *31*, 759. (b) Beletskaya, I. P.; Cheprakov, A. V. *Chem. Rev.* **2000**, *100*, 3009. (c) Cabri, W.; Candiani, I. *Acc. Chem. Res.* **1995**, *28*, 2. (d) Portnoy, M.; Ben-David, Y.; Rousso, I.; Milstein, D. *Organometallics* **1994**, *13*, 3465.

(24) Brown, J. M.; Perez-Torrente, J. J.; Alcock, N. W.; Clase, H. J. *Organometallics* **1995**, *14*, 207−213.
(25) We ruled out an unlikely radical chain mechanism because the addition of BHT (5.0 equiv) had no effect on the rate of rearrangement of **11a** to **11b**.
(26) **11a** proved unstable for extended periods of time in coordinating solvents such as CD_3CN and CD_3NO_2, probably due to gradual solvent exchange with **8**.
(27) Hansch, C.; Leo, A.; Taft, R. W. *Chem. Rev.* **1991**, *91*, 165.
(28) Roy, A.; Hartwig, J. F. *J. Am. Chem. Soc.* **2001**, *123*, 1232.
(29) The chemical shift very close to that of **28a** suggests this species may be the iodide dissociated complex.
(30) Fors, B. P.; Buchwald, S. L. *J. Am. Chem. Soc.* **2010**, *132*, 15914.
(31) (a) Barder, T. E.; Biscoe, M. R.; Buchwald, S. L. *Organometallics* **2007**, *26*, 2183. (b) Biscoe, M. R.; Barder, T. E.; Buchwald, S. L. *Angew. Chem., Int. Ed.* **2007**, *46*, 7232.
(32) Burgo, C. H.; Barder, T. E.; Huang, X. H.; Buchwald, S. L. *Angew. Chem., Int. Ed.* **2006**, *45*, 4321.
(33) Despite numerous attempts, we were never able to obtain an oxidative addition complex of **6**, the bulkiest known di-*tert*-butyl biaryl phosphine ligand.
(34) While more electron-rich Pd(II) complexes are more tilted with *t*BuBrettPhos than the corresponding electron-deficient complexes, the same trend does not hold true across all ligand classes (namely *t*BuXPhos).
(35) Yihan, S.; et al. *Phys. Chem. Chem. Phys.* **2006**, *8*, 3172.
(36) (a) Hay, P. J.; Wadt, W. R. *J. Chem. Phys.* **1985**, *82*, 270. (b) Wadt, W. R.; Hay, P. *J. Chem. Phys.* **1985**, *82*, 284. (c) Hay, P. J.; Wadt, W. R. *J. Chem. Phys.* **1985**, *82*, 299.
(37) Hehre, W. J.; Ditchfield, R.; Pople, J. A. *J. Chem. Phys.* **1972**, *56*, 2257.
(38) Perdew, J. P.; Burke, K.; Ernzerhof, M. *Phys. Rev. Lett.* **1996**, *77*, 3865.
(39) The approximation that $\Delta G \approx \Delta E$ was made in order to simplify the DFT calculations.
(40) Neglecting the CHO outlier yields $\rho = 2.48 \pm 0.24$ and a linear fit with $R^2 = 0.94909$.
(41) Companion, A. L.; Komarynsky, M. A. *J. Chem. Educ.* **1964**, *41*, 257.
(42) For a second-row transition element such as Pd, electron correlation and spin−orbit effects are generally weak relative to crystal field splittings and so can be neglected. See: Figgis, B. N., Ligand Field Theory. In *Comprehensive Coordination Chemistry*; Wilkinson, G., Gillard, R. D., McCleverty, J. A., Eds.; Pergamon: Oxford, U.K., 1987; Vol. *1*, Chap. 6, pp 213−279.
(43) Fukui, K. *J. Phys. Chem.* **1970**, *74*, 4161.
(44) The optimized structures of all intermediates and transition states shown in Figure 18 were found by starting from those found for the rearrangement of **11a** and re-optimizing the geometries, as a crystal structure of **12b** could not be obtained.
(45) Cooling an NMR sample (CD_2Cl_2, 20 to −50 °C) of **12a** revealed no interconverting species to be present. Although this result could be consistent with the interchange between **12a** and **12a′** being so facile as to be undetectable even at −50 °C, we believe this is highly unlikely and that it is more likely that **12a′** forms in only trace amounts in solution.